Morphological Characterization of the Retina of the CNGA3$^{-/-}$Rho$^{-/-}$ Mutant Mouse Lacking Functional Cones and Rods

Ellen Claes,[1] *Mathias Seeliger,*[2] *Stylianos Michalakis,*[3] *Martin Biel,*[3] *Peter Humphries,*[4] *and Silke Haverkamp*[1]

Purpose. To assess the structural changes in the retina caused by a functional blockade of rods and cones and to document the time course of their degeneration.

Methods. Double knockout mice were generated by cross-breeding CNGA3$^{-/-}$ mice with Rho$^{-/-}$ mice. Retinas of mutant and wild-type mice from 3 weeks up to 12 months of age were studied by confocal light and electron microscopy. The retinas were immunostained with cell-type–specific markers and with antibodies against synapse-associated proteins and transmitter receptors.

Results. In 3-week-old CNGA3$^{-/-}$Rho$^{-/-}$ mice, retinal layers showed normal structural organization, and photoreceptors established normal synaptic contacts. Until postnatal week (Pw)7, presynaptic markers and postsynaptic glutamate receptors were well expressed at the photoreceptor terminals. Photoreceptor degeneration started at Pw4, progressing to an almost complete loss by 3 months. Rod spherules showed an increase in the number of synaptic ribbons and postsynaptic elements during this early stage of degeneration, and horizontal cell processes grew into the outer nuclear layer. At later stages of retinal degeneration, the inner plexiform layer (IPL) was also affected. Rod bipolar cell axon terminals showed morphologic alterations, but the stratification pattern of cone bipolar cell axons and amacrine cell processes appeared unaffected. Transmitter receptors (GlyRα3, GABA$_A$ α2, GluR2/3) showed no obvious changes in the distribution and density of their synaptic clusters throughout the IPL at postnatal month 12.

Conclusions. The normal structural and synaptic organization of the mutant retina at Pw3 suggests that photoreceptor light responses are not essential for the development of the retinal circuitry. However, functional photoreceptors are necessary for the maintenance of rods and cones and their contacts in the OPL, because they degenerate almost completely by 3 months after birth. Degenerative changes can also be observed in the IPL; however, they appear to have a slower time course and by 12 months of age the IPL circuitry appears to be surprisingly intact. (*Invest Ophthalmol Vis Sci.* 2004;45:2039–2048) DOI: 10.1167/iovs.03-0741

Photoreceptor degeneration is the most common cause of inherited retinal blindness. The retinal degeneration (*rd*) mouse is a well-characterized animal model, in which a mutation of the rod-specific phosphodiesterase[1] leads to the loss of nearly all rod photoreceptors in the first 3 weeks of postnatal life. For unknown reasons, the cones are also affected and subsequently degenerate.[2] In addition, second-order neurons of the *rd* mouse show dramatic morphologic modifications after photoreceptor loss.[3,4]

Photoreceptor degeneration also develops in rhodopsin knockout (Rho$^{-/-}$) mice, but with a slower time course.[5,6] Rhodopsin, the visual pigment of the rods, starts the phototransduction cascade, but also serves as a structural protein for the discs in the rod outer segments. Therefore Rho$^{-/-}$ mice do not have rod outer segments, and they lose their photoreceptors within 3 months. Rho$^{-/-}$ mice lack any rod function, but between postnatal week (Pw)4 and Pw6, when cone degeneration is not yet substantial, these mice can be used to study pure cone function.[7]

Photoreceptors respond to light by the closure of a cyclic nucleotide-gated (CNG) cation channel in the plasma membrane, causing hyperpolarization and decrease of the synaptic glutamate release. In rod photoreceptors the CNG channel is formed by the subunits CNGA1 and CNGB1 and in cone photoreceptors by CNGA3 and CNGB3.[8] CNGA3 knockout (CNGA3$^{-/-}$) mice lack any cone-mediated photoresponses.[9] Furthermore, the cones in CNGA3$^{-/-}$ mice undergo a progressive degeneration due to unknown molecular events.

For this study, we generated double-mutant mice and investigated the degenerative changes of the retina in the absence of functional photoreceptors.

Methods

Animals

Double-mutant mice were generated by cross-breeding CNGA3$^{-/-}$ mice[9] with Rho$^{-/-}$ mice.[5] The resultant double-knockout mice in the F2 generation were identified by PCR. Wild-type (wt) mice of the same genetic background (C57BL/6) were used for comparison. The study was performed in accordance with the ARVO Statement for the Use of Animals in Ophthalmic and Vision Research.

Electroretinograms

ERGs were obtained as previously described.[10] Single-flash responses were recorded under dark-adapted (scotopic) and light-adapted (photopic) conditions. Stimuli were presented with increasing intensities,

From the [1]Department of Neuroanatomy, Max-Planck-Institute for Brain Research, Frankfurt/M, Germany; the [2]Retinal Electrodiagnostics Research Group, Department of Ophthalmology, University of Tübingen, Tübingen, Germany; the [3]Institute of Pharmacology, Center for Drug Research, Ludwig-Maximilian University, Munich, Germany; and the [4]Department of Genetics, Trinity College, The University of Dublin, Ireland.

Supported by Deutsche Forschungsgemeinschaft Grant SFB 269/B4.

Submitted for publication July 16, 2003; revised October 14, 2003 and January 26, 2004; accepted February 22, 2004.

Disclosure: **E. Claes**, None; **M. Seeliger**, None; **S. Michalakis**, None; **M. Biel**, None; **P. Humphries**, None; **S. Haverkamp**, None

The publication costs of this article were defrayed in part by page charge payment. This article must therefore be marked "*advertisement*" in accordance with 18 U.S.C. §1734 solely to indicate this fact.

Corresponding author: Silke Haverkamp, Max-Planck-Institute for Brain Research, Department of Neuroanatomy, Deutschordenstrasse 46, D-60528 Frankfurt/M, Germany;
haverkamp@mpih-frankfurt.mpg.de.

TABLE 1. Sources and Working Dilutions of Antibodies

Antigen	Antiserum, Working Dilution	Source
Bassoon	Mouse anti-bassoon, 1:5000	StressGen Biotechnologies, Victoria, BC, Canada
GluR1	Rabbit anti-GluR1, 1:100	Chemicon International Inc., Temecula, CA
GluR5	Goat anti-GluR5 (N-19), 1:100	Santa Cruz Biotechnology, Santa Cruz, CA
mGluR6	Rabbit anti-mGluR6, 1:1000	Neuromics, Minneapolis, MN
α1F	Sheep anti-α1F, 1:1000	C. Morgans, OHSU, Beaverton, OR[15]
PMCA1	Rabbit anti-PMCA1, 1:300	A. G. Filoteo, Rochester, NY[38]
Calbindin	Rabbit anti-calbindin, 1:2000	Swant, Bellinzona, Switzerland
PKCα	Mouse anti-PKCα, clone MC5, 1:100	Amersham, Arlington Heights, IL
Disabled-1	Rabbit anti-disabled-1, 1:500	B. W. Howell, NIH, Bethesda, MD[39]
Calretinin	Rabbit anti-calretinin, 1:2000	Swant, Bellinzona, Switzerland
CaB5	Rabbit anti-CaB5, 1:500	K. Palczewski, Seattle, WA[20]
Kinesin II	Mouse anti-kinesin II, 1:50	Babco, Richmond, CA
VGAT	Guinea pig anti-VGAT, 1:5000	Chemicon International Inc.
$GABA_A$ α2	Guinea pig anti-$GABA_A$ α2, 1:2000	H. Möhler, Zürich, Switzerland[40]
GlyR α3	Rabbit anti-GlyR α3, 1:1000	R. J. Harvey, London, UK[27]
GluR2/3	Rabbit anti-GluR2/3, 1:100	Chemicon International Inc.

reaching from 10^{-4} cd · s/m^2 to 25 cd · s/m^2, divided into 10 steps. Ten responses were averaged with an inter-stimulus interval (ISI) of 5 seconds (for 0.1, 1, 10, 30, 100, 300 mcd · s/m^2), 10 seconds (for 1 and 3 cd · s/m^2), or 20 seconds (for 10 and 25 cd · s/m^2).

Histology

Immunocytochemistry. CNGA3$^{-/-}$Rho$^{-/-}$ double-mutant mice of different ages (Pw3–12, postnatal months [Pm]9–12) and wt mice of the same ages were deeply anesthetized with halothane (4% in oxygen) and decapitated. The eyes were enucleated, the anterior segments removed, and the posterior eyecups immersion fixed for 10 to 15 minutes in 4% paraformaldehyde in 0.1 M phosphate buffer (pH 7.4) at room temperature. For studying transmitter receptor staining in the IPL, the fixation time was reduced to 5 minutes. Due to the reduced thickness of the mutant retina at Pm9 or later (half the thickness of normal retina) fixation-sensitive antibodies did not work on tissue fixed longer than 5 minutes. After fixation, the retinas were dissected from the eyecup, cryoprotected in graded sucrose solutions (10%, 20%, and 30%) and sectioned vertically at 14 μm with a cryostat. In some experiments, wholemounted retinas were used.

Immunocytochemical labeling was performed by the indirect fluorescence method. The sources and working dilutions of antibodies are listed in Table 1. Sections were incubated overnight with primary antibodies diluted in 5% chemiblocker (Chemicon, Hofheim, Germany) and 0.5% Triton X-100 in phosphate-buffered saline (PBS, pH 7.4). After the sections were washed in PBS, secondary antibodies were applied for 1 hour. These were conjugated to either Alexa 594 (red fluorescence) or Alexa 488 (green fluorescence; Molecular Probes, Eugene, OR). In double-labeling experiments, sections were incubated in a mixture of primary antibodies followed by a mixture of secondary antibodies.

Fluorescent specimens were viewed with a microscope (Axiophot; Carl Zeiss Meditec, Oberkochen, Germany). Digital images were taken with a cooled charge-coupled device (CCD) camera (Spot 2; Diagnostic Instruments, Sterling Heights, MI). Confocal micrographs were taken with a confocal microscope (LSM5 Pascal; Carl Zeiss Meditec) equipped with an argon (Ar) laser and a helium-neon (HeNe) laser. Brightness and contrast of the final images were adjusted by computer (Photoshop 6.0; Adobe, San Diego, CA).

Electron Microscopy. For optimal tissue preservation, posterior eyecups were immersion-fixed for 1 hour in a mixture of 4% paraformaldehyde and 2% glutaraldehyde in 0.1 M cacodylate buffer. After the retina was isolated and dissected into small blocks, tissue was postfixed with osmium tetroxide, stained en bloc with uranyl acetate, dehydrated in ethanol, and embedded in Epon 812. Semithin sections were stained with toluidine blue. Ultrathin sections were viewed with an electron microscope (EM10; Carl Zeiss Meditec).

For comparing the synaptic organization in the outer plexiform layer (OPL) of the CNGA3$^{-/-}$Rho$^{-/-}$ mutant retina with the wt retina, counts were made of rod terminals and their synaptic ribbons at Pw4,

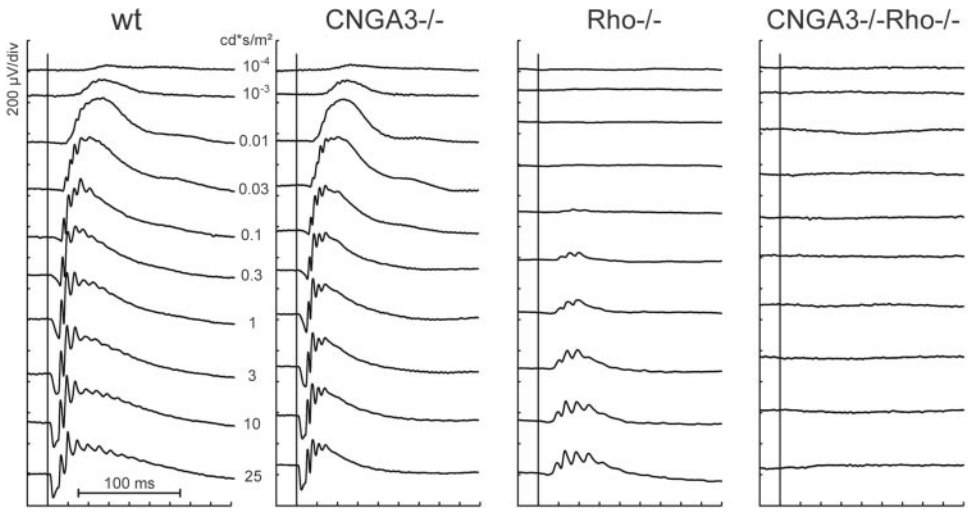

FIGURE 1. Records of scotopic ERGs from wt, CNGA3$^{-/-}$, Rho$^{-/-}$, and CNGA3$^{-/-}$Rho$^{-/-}$ mice at approximately P35. No discernible rod or cone-driven responses were obtained from the double-mutant mice.

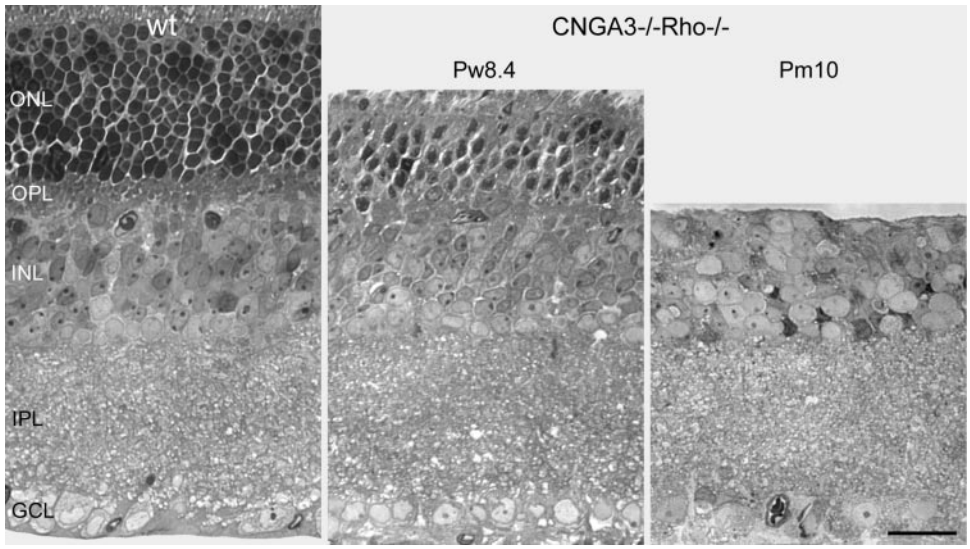

FIGURE 2. Toluidine blue-stained vertical semithin section of a wt mouse retina compared to retinal sections of CNGA3$^{-/-}$Rho$^{-/-}$ mice at Pw8.4 and Pm10. The mutant retina showed a massive reduction of the outer nuclear layer (ONL) at Pw8.4, whereas the inner retina appeared unaffected. At Pm10 the outer retina appeared to have degenerated completely, whereas the inner retina did not show substantial morphologic changes. OPL, outer plexiform layer; INL, inner nuclear layer; IPL, inner plexiform layer; GCL, ganglion cell layer. Scale bar, 25 μm.

Pw5, and Pw6. Sections, 450 to 900 μm wide, were analyzed from one end to the other. Only rod terminals with at least one synaptic ribbon and two postsynaptic elements were included, profiles without synaptic elements were excluded. Rod terminals with one and those with two or more synaptic ribbons were separately counted and compared as a percentage of the total.

RESULTS

Recordings of the ERG

In the CNGA3$^{-/-}$Rho$^{-/-}$ mouse, no discernible ERG responses from the rod or the cone system were recordable. Figure 1 illustrates this finding for the scotopic ERG in comparison to the single knockout and wt mice. The photopic ERG confirmed the lack of cone function (not shown).

Photoreceptor Degeneration

In the CNGA3$^{-/-}$Rho$^{-/-}$ mouse, progressive photoreceptor degeneration takes place in the first 3 months after birth. After 3 weeks, when maturation of the mouse retina is essentially complete, the retinal layers of the mutant mouse appeared normally developed, only the rod outer segments were missing (not shown). With 2 months, a massive reduction of the outer nuclear layer (ONL) was evident, but the inner retina appeared unaffected (Fig. 2, Pw8.4). The same was true for a 10-month-old mutant retina. Although the photoreceptors had been completely degenerated for months, the gross morphology, such as the thickness of the inner retinal layers, was still comparable to that of the wt retina (Fig. 2, Pm10).

Figure 3 shows the progression of the photoreceptor degeneration in more detail. Loss of cells in the ONL started at about Pw4. Mutant mice had 8 to 10 rows of photoreceptor nuclei compared with 10 to 12 rows in wt mice. Between Pw7 and Pw8, loss of cells increased significantly, at Pw10, the photoreceptor layer was reduced to one row of nuclei, and at Pw12, the entire ONL was gone in most parts of the retina.

Synaptic Changes in the OPL

The synaptic contacts between photoreceptor terminals, horizontal cell processes, and bipolar cell dendrites appeared relatively normal in the CNGA3$^{-/-}$Rho$^{-/-}$ retina until Pw4. Rod spherules with one triad synapse (Fig. 4A) and cone pedicles with multiple triad synapses were found the same as in wt retina. However, quantitative electron microscopic analysis showed that by Pw4, the number of the rod spherules has already decreased to less than half of the wt number (Table 2). We also found rod spherules with two, three, or more synaptic ribbons and larger numbers of postsynaptic elements. At Pw4, 45% of the rod spherules contained two or more ribbons in the mutant, whereas in the wt, only 4% had more than one ribbon. At Pw5 and Pw6, even more than 80% of the surviving rod spherules had two or more ribbons (Table 2).

An antibody against the cytomatrix protein bassoon[11] was used to label the presynaptic ribbon complex in rod spherules and cone pedicles and to follow their extensive

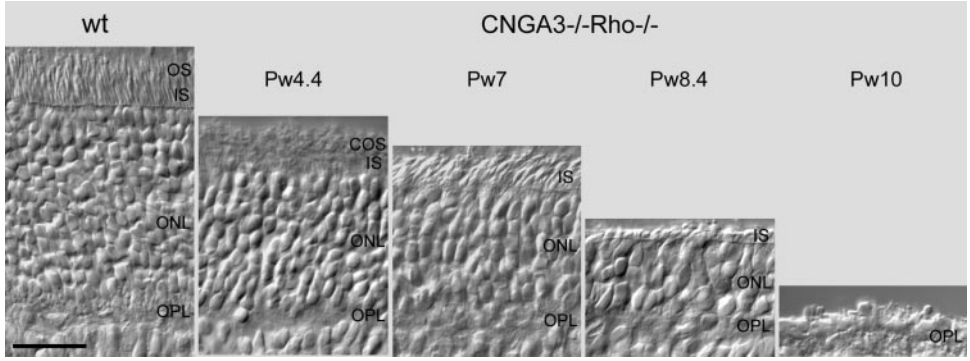

FIGURE 3. Nomarski micrographs showing the outer retina of a wt mouse in comparison to retinas of CNGA3$^{-/-}$Rho$^{-/-}$ mice of different postnatal ages. Photoreceptor degeneration started at approximately Pw4 and increased drastically after Pw7; at Pw10, only scattered nuclei were left. OS, photoreceptor outer segments; IS, photoreceptor inner segments; COS, cone outer segments; ONL, outer nuclear layer; OPL, outer plexiform layer. Scale bar, 25 μm.

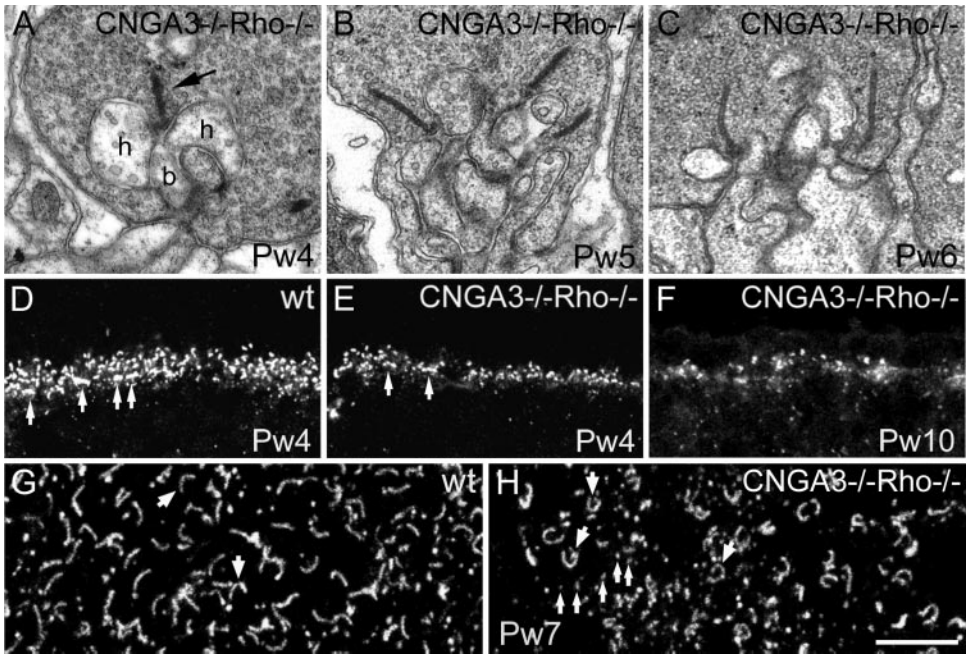

FIGURE 4. Synaptic changes in the OPL. (**A–C**) Electron micrographs of vertical sections through rod spherules of CNGA3$^{-/-}$Rho$^{-/-}$ retinas. At Pw4 (**A**) many of the rod spherules showed a normal triad synaptic complex with a presynaptic ribbon (*arrow*) and three postsynaptic elements, two horizontal cell processes (h), and a rod bipolar cell dendrite (b). At Pw5 (**B**) and Pw6 (**C**) an increase in the number of synaptic ribbons and postsynaptic elements in most of the surviving rod spherules was observed (Table 2). (**D–F**) Confocal fluorescence micrographs of vertical sections from wt and CNGA3$^{-/-}$ Rho$^{-/-}$ retinas showing the progressive degeneration of rod terminals in the OPL at the light microscopic level. The synaptic ribbons were visualized with an antibody against the cytomatrix protein bassoon, which labels photoreceptor ribbons in both cone pedicles and rod spherules. In wt retina (**D**), four to six rows of bassoon labeling was normally seen, equivalent to the rows of rod spherules, and a clustering of bassoon at cone pedicles is visible (*arrows*). In the mutant at Pw4 (**E**) the clustering of ribbon synapses at cone pedicles was obvious (*arrows*), but the number of bassoon-labeled ribbons in rod spherules had already decreased. At Pw10 (**F**) only a few puncta of bassoon labeling remained. (**G**, **H**) Wholemount view of bassoon labeling to demonstrate the different size and structure of the synaptic ribbons in wt and CNGA3$^{-/-}$Rho$^{-/-}$ retinas at Pw7. The characteristic horseshoelike appearance of a synaptic ribbon in a rod spherule (**G**, *arrows*) turns into a ring-shaped (**H**, *arrows*) or punctate structure (**H**, *small arrows*). Scale bar: (**A–C**) 0.54 μm; (**D–F**) 19 μm; (**G**, **H**) 5 μm.

degeneration at the light microscopic level. In wt retina, four to six rows of bassoon-labeled ribbons were present, equivalent to the four to six rows of rod spherules, and a clustering of bassoon at cone pedicles was apparent (Fig. 4D). In the mutant mouse at Pw4, the number of bassoon-labeled ribbons had already decreased, and by Pw10, only a few bassoon-labeled puncta were left (Figs. 4E, 4F). In addition, the characteristic horseshoelike appearance of the bassoon-labeled ribbons turned into ring-shaped structures during the process of degeneration and disappeared at later stages (Figs. 4G, 4H).

Localization of GluR1, mGluR6, α1F, and PMCA1 at the Photoreceptor Terminals

We were interested in whether synapse-associated proteins and postsynaptic glutamate receptors aggregate at the photoreceptor terminals in the absence of rod and cone light signaling. In wt mice, the glutamate receptor subunit GluR1 has been shown to be expressed on the dendritic tips of putative OFF bipolar cells making flat contacts at the cone pedicle base.[12] The wholemount view in Figures 5A and 5A′ demonstrates a high expression of GluR1 at the cone pedicles (circles) of both the wt and the CNGA3$^{-/-}$Rho$^{-/-}$ retinas. The only difference we found in the mutant retina was a delayed expression of approximately 1 week. The metabotropic glutamate receptor of invaginating ON bipolar cells, mGluR6,[13,14] was well expressed at both rod spherules (frame, Fig. 5B′) and cone pedicles in CNGA3$^{-/-}$ Rho$^{-/-}$ retinas. The same holds true of the calcium channel subunit α1F and the plasma membrane calcium adenosine triphosphatase (ATPase 1; PMCA1). Both have been localized to rod spherules and cone pedicles in rodent retina[15,16] and both were expressed in the CNGA3$^{-/-}$ Rho$^{-/-}$ mouse (Figs. 5C′, 5D′), indicating that glutamate release and calcium extrusion could take place.

Changes in Second-Order Neurons

Immunofluorescence labeling using selective cell markers, such as calbindin for horizontal cells and protein kinase-Cα (PKCα) for rod bipolar cells,[17] revealed a sprouting of their processes into the ONL between Pw4 and Pw7. Figures 6A and 6A′ show a comparison of calbindin-labeled horizontal cells in wt and CNGA3$^{-/-}$Rho$^{-/-}$ retinas at Pw5. In wt retina, the horizontal cell processes formed a regular and dense plexus, whereas in the mutant retina, many of the horizontal cell processes extended far into the outer as well

TABLE 2. Changes in the Number of Rod Photoreceptor Terminals and Synaptic Ribbons in the OPL of Wt and CNGA3$^{-/-}$Rho$^{-/-}$ Mutant Mice at Different Ages

	Wt Pw4	Mutant Pw4	Mutant Pw5	Mutant Pw6
Total number of terminals per 1000 μm	337	157	90	70
Terminals containing 1 ribbon	323 (96)	86 (55)	15 (17)	11 (16)
Terminals containing 2 or more ribbons	14 (4)	71 (45)	75 (83)	59 (84)

Data for terminals containing ribbons are the number of terminals with the percentage in parentheses.

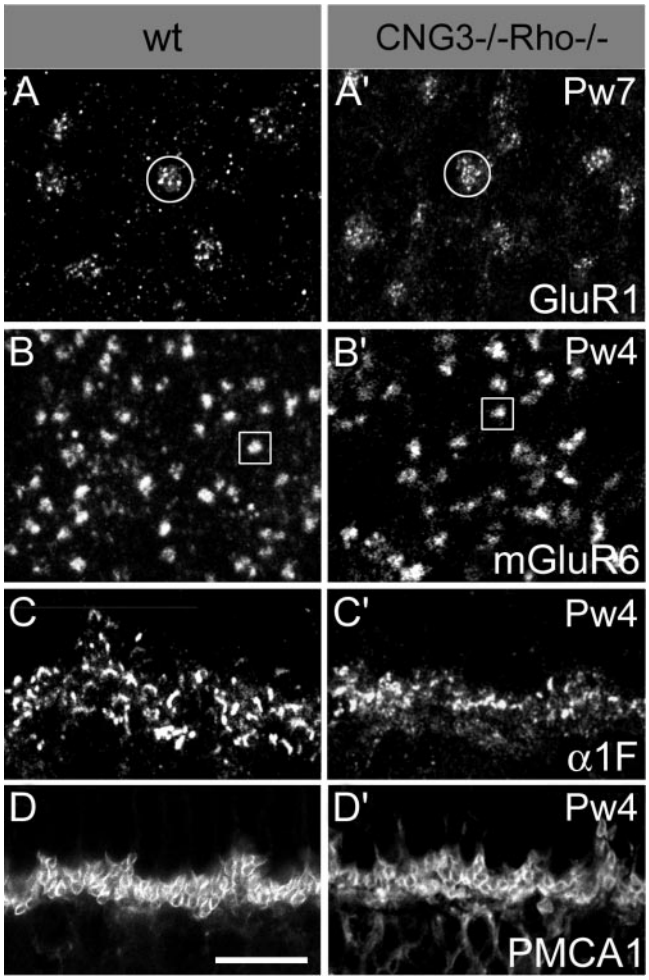

FIGURE 5. Glutamate receptor localization at the photoreceptor terminals of wt (*left*) and CNGA3$^{-/-}$Rho$^{-/-}$ mice (*right*). (**A**, **A′**) Wholemount view of GluR1 expression at cone pedicles (*circles*) in wt and CNGA3$^{-/-}$Rho$^{-/-}$ retinas at Pw7. GluR1 was expressed on dendrites of OFF bipolar cells, making flat contacts at the cone pedicle base, and seemed to be normally expressed in mutant mice. (**B**, **B′**) Wholemount view of the expression of the ON bipolar cell receptor mGluR6 showing punctate labeling at rod spherules (framed) in both wt and CNGA3$^{-/-}$Rho$^{-/-}$ animals at Pw4. (**C**, **C′**) α1F calcium channel subunit expression on vertical sections. In wt retina α1F appeared concentrated at the active zone of the synaptic ribbon complex in horseshoelike structures similar to bassoon labeling. In the CNGA3$^{-/-}$Rho$^{-/-}$ mouse at Pw4, α1F expression was visible but slightly reduced. (**D**, **D′**) Staining pattern of the plasma membrane calcium ATPase isoform PMCA1 on vertical sections. In wt retina, PMCA1 was localized to rod spherules and cone pedicles and was mainly responsible for the Ca^{2+} extrusion into the OPL. The CNGA3$^{-/-}$Rho$^{-/-}$ mouse at Pw4 also shows expression, but not as strong as in wt. Scale bar: (**A**, **A′**) 15 μm; (**B**, **B′**) 5 μm; (**C**, **C′**, **D**, **D′**) 10 μm.

as the inner nuclear layer (INL). We observed similar morphologic changes in the Rho$^{-/-}$ retina (Fig. 6B), and double-labeling experiments with calbindin and bassoon showed that the outgrowing horizontal cell processes were in contact with ectopic photoreceptor ribbons (Figs. 6B, 6B′, circles).

After 3 months, dendrites of rod and cone bipolar cells and thin processes of horizontal cells had mostly retracted (not shown).

Morphologic Changes in the Rod Bipolar Cell Axon Terminals at Later Stages of Retinal Degeneration

To analyze possible long-term changes in the inner retina of CNGA3$^{-/-}$Rho$^{-/-}$ mice after total loss of photoreceptors, 9 to 12-month-old animals were investigated. The coarse structure of the inner retina was not affected significantly in the mutant (Fig. 2, Pm10); however, the axon terminals of rod bipolar cells showed dramatic alterations at Pm9 (Fig. 7). In the wt retina, PKCα-labeled rod bipolar cell axons terminated in lobular varicosities at the inner margin of the IPL (Fig. 7A). In the mutant at Pw4, axon terminals and ribbon synapses of rod bipolar cells were normally developed (Figs. 7A′, 7C′) and did not show any alterations at least until Pw7. At later stages of retinal degeneration, however, some of the terminals had retracted and some of them appeared swollen compared with wt terminals (Fig. 7A″). Double labeling with PKCα and antibodies against the ribbon marker kinesin[18] demonstrated that ribbons were more or less absent from the swollen rod bipolar cell terminals (data not shown), and by electron microscope, only rudimentary ribbon synapses were visible (Fig. 7C″).

In contrast, the rod bipolar–driven AII amacrine cells (which can be labeled in mouse retina with an antibody against disabled 1[19]) showed no striking alterations in the mutant retina at all the ages tested (Figs. 7B, 7B′, 7B″).

Fine Structure of the IPL: Stratification Pattern and Distribution of Synapses

Antibodies against the calcium-binding proteins calretinin and CaB5 have been used to analyze the stratification pattern within the IPL (Fig. 8). Calretinin immunofluorescence reveals the perikarya of many amacrine cells, displaced amacrine cells and ganglion cells, and three strata of dense processes within the IPL, the two cholinergic bands and one band in the center of the IPL.[17] The staining pattern of the IPL of a 12-month-old mutant mouse was similar to the wt retina. Three bands of processes were visible, only the space between band 3 and the GCL, where the rod bipolar cells terminate, was reduced. The cell bodies appeared more strongly labeled in the mutant retina (Figs. 8A, 8A′). CaB5 stains three distinct layers of bipolar cell axon terminals in the IPL, representing three distinct bipolar cell types.[20,21] The staining pattern of the OFF- and ON-cone bipolar cell axon terminals was comparable in wt and mutant retinal sections (Figs. 8B, 8B′), but the axon terminals of the rod bipolar cells showed some alterations, which were described in detail in the previous section.

Antibodies against kinesin have been used to visualize the bipolar cell ribbon synapses in the IPL (Figs. 8C, 8C′). The immunofluorescence revealed punctate staining throughout the IPL, and no difference was detectable between wt and mutant retina, except for a decreased staining pattern in the innermost IPL of the mutant where the rod bipolar cells terminate (see previous section). This suggests that the output synapses of the cone bipolar cells were not yet affected in the mutant retina. These findings were supported by electron microscopic data showing perfect ribbon synapses in axon terminals of ON- and OFF-cone bipolar cells in CNGA3$^{-/-}$Rho$^{-/-}$ mice (Fig. 8D).

For immunostaining amacrine cell processes, we used an antibody against the vesicular γ-aminobutyric acid (GABA)/glycine transporter (VGAT).[22] VGAT immunoreac-

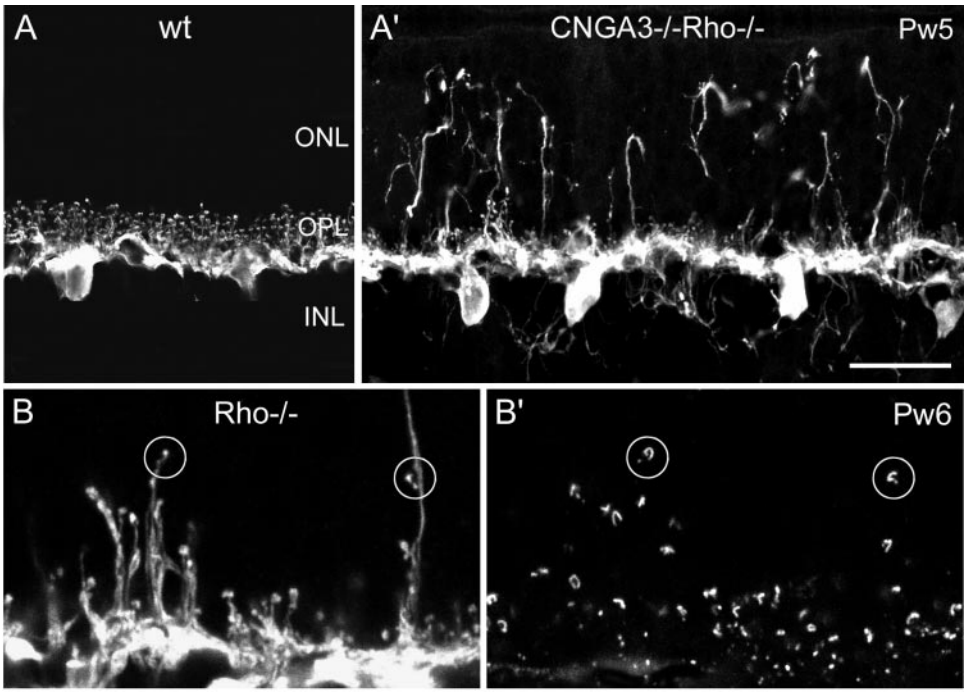

FIGURE 6. Horizontal cell sprouting and ectopic ribbon synapses in the ONL. (**A**, **A′**) Confocal micrographs of horizontal cell labeling in wt and CNGA3$^{-/-}$Rho$^{-/-}$ mouse at Pw5, visualized by calbindin immunocytochemistry. In the mutant retina, horizontal cell processes show extensive sprouting into the ONL and INL. (**B**, **B′**) Double labeling for calbindin (**B**) and bassoon (**B′**) on a vertical section of a Rho$^{-/-}$ retina at Pw6. The *circles* enclose two examples where outgrowing horizontal cell processes (**B**) are in contact with presynaptic photoreceptor ribbons (**B′**). Scale bar: (**A**, **A′**) 25 μm; (**B**, **B′**) 9.5 μm.

tivity was strong in all laminae of the IPL and no significant difference was observed between wt and mutant mice (Figs. 8E, 8E′). We found no difference in the ultrastructure of conventional synapses (Fig. 8F); however, we had the impression that the number of amacrine cell synapses was increased. Although we have no statistical data on this, an increased number of conventional synapses would fit with quantitative electron microscopic data from light-deprived retinas.[23,24]

Distribution of Inhibitory and Excitatory Transmitter Receptors within the IPL

It has been shown that the clustering of transmitter receptors in postsynaptic densities is a dynamic, activity-dependent process.[25,26] Because pathologic changes in the retina may cause redistribution and a possible deaggregation of transmitter receptors, it was important to investigate the expression level and the clustering of the different receptors in the CNGA3$^{-/-}$Rho$^{-/-}$ retina. Glutamate is the major excitatory transmitter of the retina, and GABA and glycine are the major inhibitory transmitters. Molecular cloning has shown that the receptors to which these transmitters bind consists of multiple subunits, and these subunits exhibit distinct patterns of stratification in the IPL and are clustered in different synapses (for normal mouse retina, see Ref. 17). We tested a variety of receptor types in the CNGA3$^{-/-}$Rho$^{-/-}$ mouse, and all of them showed the same pattern of distribution as observed in wt retina. This was true in retinas of mutant mice at Pw4 (not shown); however, we were surprised to find a comparable clustering of transmitter receptors in 12-month-old mice as well (Fig. 9), when all photoreceptors had long since degenerated. The α2 subunit of the $GABA_A$ receptor, for example, showed two distinct bands of higher density at the cholinergic strata (Figs. 9A, 9A′), whereas the GlyR α3 subunit showed punctate labeling in four characteristic bands (Fig. 9B, 9B′).[27] Immunoreactive puncta of the glutamate receptor subunit GluR2/3 were found at high density throughout the IPL, except for the innermost layer in mutant retina where the rod bipolar axon terminals were partially retracted (Fig. 9C, 9C′).

In addition, in rare cases, dislocated receptor clustering associated with sprouting bipolar and ganglion cell processes showed up in the INL (not shown) which might be comparable to the microneuromas (new foci of synaptic neuropil) recently described in different photoreceptor degeneration models.[28]

DISCUSSION

By cross-breeding CNGA3$^{-/-}$ and Rho$^{-/-}$ animals, we were able to obtain mice without any photoreceptor light responses throughout their entire lifespan. The lack of such function was verified by electroretinography (ERG). The question we wanted to answer with these mice was how the other more downstream parts of the retina would react to never receiving any light-driven input from photoreceptors.

We found that CNGA3$^{-/-}$Rho$^{-/-}$ double-mutant mice show a progressive degeneration of all photoreceptors within 3 months after birth. However, throughout the first weeks of life, until Pw7, presynaptic markers and postsynaptic glutamate receptors are well expressed in the OPL, suggesting neurotransmission could take place. This indicates that photoreceptor light responses are not essential for the structural development of their output synapses after eye opening.

During the first weeks of photoreceptor degeneration, some of the surviving rod spherules showed an increase in the number of their synaptic ribbons and postsynaptic elements. This kind of synaptic plasticity in rod spherules after partial photoreceptor loss has been reported in *rds* mutant mice[29] and in light-damaged albino mice[30] and has been interpreted as a reaction to the reduction of afferent input to the postsynaptic components.

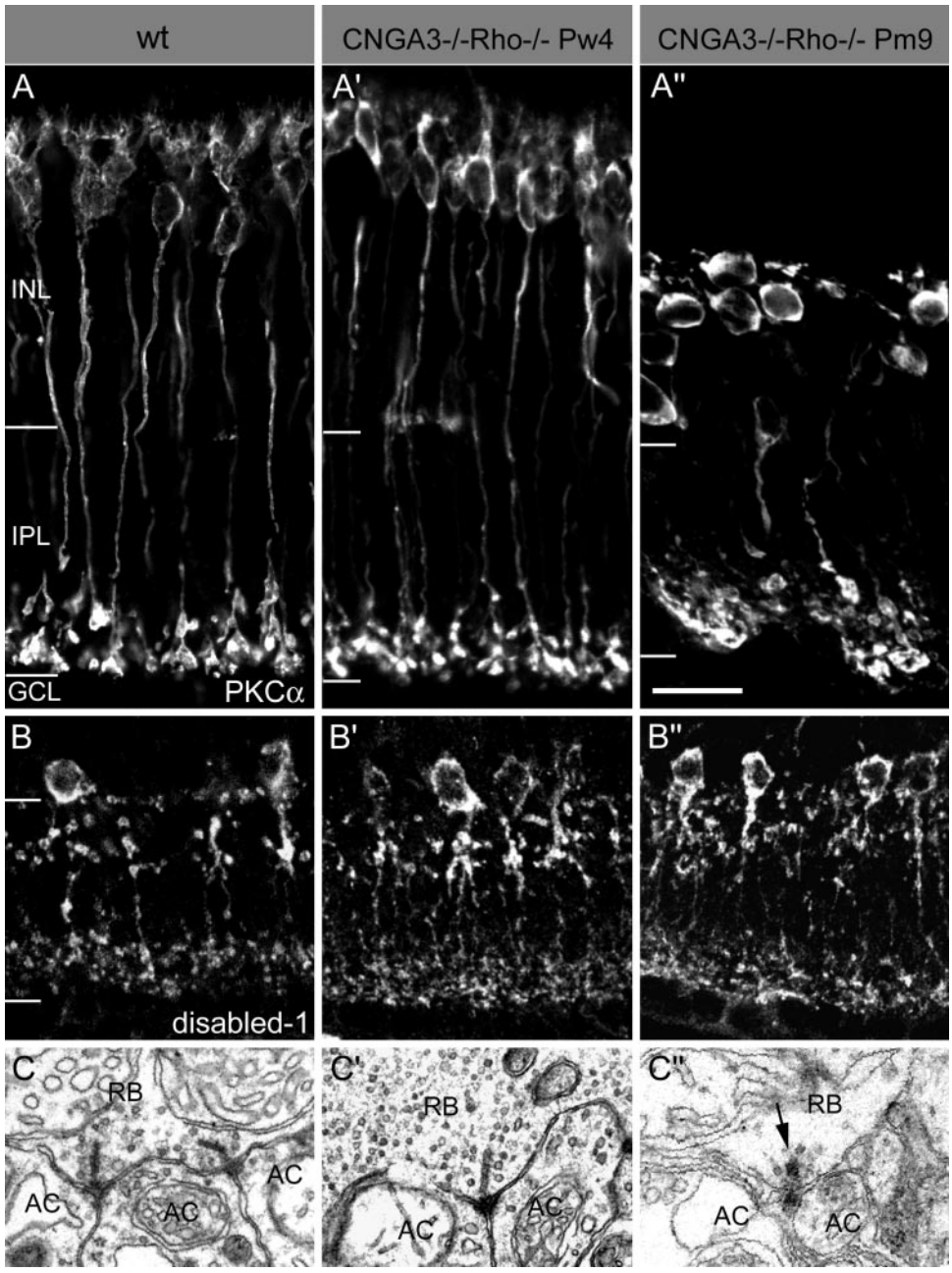

FIGURE 7. Effects of retinal degeneration on the rod pathway. A comparison of rod bipolar and AII amacrine cell morphology in wt retina (**A–C**) and CNGA3$^{-/-}$Rho$^{-/-}$ retinas at Pw4 (**A′–C′**) and Pm9 (**A″–C″**). (**A**) Confocal images of vertical sections immunostained for PKCα. The inner and outer borders of the IPL are marked by *white lines*. PKCα-stained rod bipolar cells. Their cell bodies were found in the outer INL, and their axons terminated in the inner IPL, close to the GCL. The axon terminals were normally developed in the mutant retina at Pw4 (**A′**), but showed morphologic changes at Pm9 (**A″**). It seems that some of the varicosities were fused together, and some of them retracted into the middle of the IPL. (**B**) AII amacrine cell morphology was visualized with antibodies against disabled-1. AII cells had bistratified dendritic trees that spanned both the outer and inner halves of the IPL. Their morphology appeared normal in the mutant at both stages. (**C**) Electron micrographs of rod bipolar cell synaptic endings. Rod bipolar cells (RB) normally target amacrine cells (AC) at ribbon synapses. The long presynaptic ribbons in wt (**C**) and mutant RB terminals at Pw4 (**C′**) appeared small and spherical in the mutant at Pm9 (**C″**, *arrow*). Scale bar: (**A–A″**, **B–B″**) 20 μm; (**C–C″**) 0.53 μm.

The phenomenon that horizontal and rod bipolar cell processes grow into the ONL, where they form ectopic synapses with rod photoreceptors, has not been described in a photoreceptor-degeneration model before. But similar findings have been made in totally different models, such as in a mutant mouse retina deficient of functional bassoon[31] and in cat retina after retinal detachment.[32] However, the molecular mechanisms mediating neurite outgrowth and the genesis of ectopic synapses in these diverse animal models are unknown.

Nine-month-old CNGA3$^{-/-}$Rho$^{-/-}$ mouse retinas showed degenerative changes of rod bipolar axon terminals and of their output synapses. In contrast, the cone pathway in the IPL appeared to be mostly unchanged until Pm12. It is possible that this only reflects the different time course of the degeneration of rods and cones. Rods disappear first; therefore, the secondary degeneration within the rod pathway is expected to occur earlier. Cones degenerate later and it is possible that the secondary degenerative changes in the IPL occur only later than the 12 months we have studied so far. It is known that retinal remodeling starts at about postnatal day 200 to 600, depending on the degeneration model,[33] so we expect to find more severe defects in the inner retina of our mutant mice at later stages of degeneration.

Nevertheless, the finding of a preservation of inner retinal cells and connectivity is an important prerequisite for the success of therapeutic strategies in degenerative retinopathies like gene therapy,[34] photoreceptor transplantation,[35] or technical implants, which focus mostly on the restoration of outer retinal function. It remains to be shown whether cortical structures also keep sufficient plasticity to make use of such restored signals.

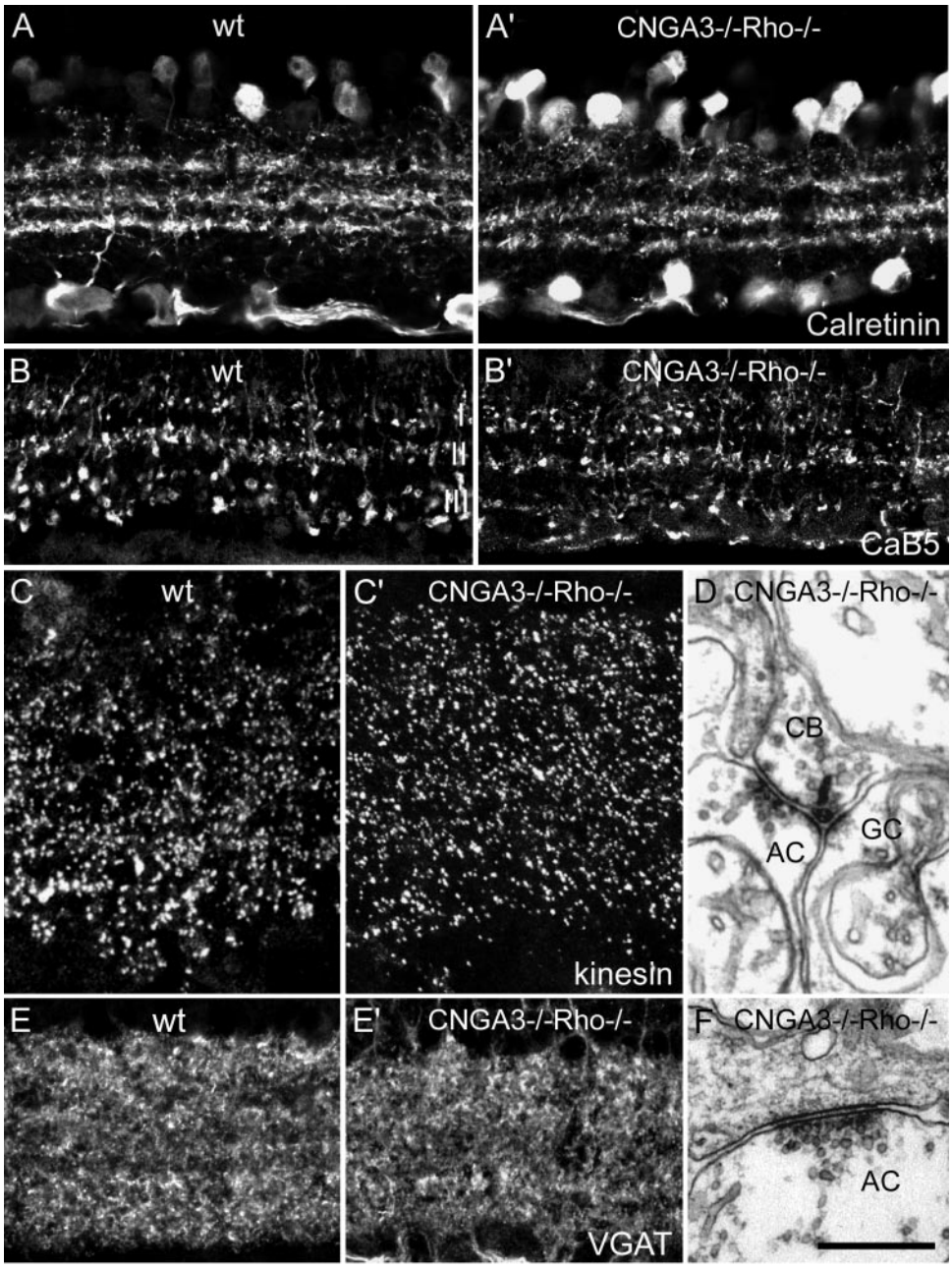

FIGURE 8. Stratification pattern and synaptic structure of the IPL of a 12-month-old CNGA3$^{-/-}$Rho$^{-/-}$ mouse in comparison to the retina of a wt mouse. (**A**,**A′**) Confocal micrographs of vertical sections immunostained for calretinin. In both wt and CNGA3$^{-/-}$Rho$^{-/-}$ retinas, three bands of dense processes within the IPL as well as the perikarya of many amacrine cells and cells in the GCL were labeled; but the space between the third band and the GCL, where the rod bipolar cells terminate, was reduced in the mutant. (**B**, **B′**) CaB5 immunostaining in the IPL of wt and CNGA3$^{-/-}$Rho$^{-/-}$ retinas. Three distinct layers of bipolar cell axon terminals can be seen, representing three different bipolar cell types: an OFF- and an ON-cone bipolar cell and the rod bipolar cells. The axon terminals of the OFF- (layer I) and ON- (layer II) cone bipolar cells showed no morphologic difference compared with the wt retina, whereas the large varicose endings of the rod bipolar cells in the wt (**B**, layer III) appeared clearly reduced in size and number in the knockout retina (**B′**, layer III). (**C**, **C′**) Kinesin immunolabeling in the IPL of vertical wt and CNGA3$^{-/-}$Rho$^{-/-}$ retinal sections. Kinesin was used as a bipolar cell ribbon marker, and no difference was seen between wt and mutant retina, except for the decreased density of ribbons in the innermost IPL of the knockout mouse in which the rod bipolar cells terminated. (**D**) Electron micrograph of CNGA3$^{-/-}$Rho$^{-/-}$ retina showing a classic ribbon synapse of a cone bipolar cell (CB) with two postsynaptic elements, possibly an amacrine cell (AC) and a ganglion cell (GC). (**E**, **E′**) Confocal images of VGAT immunolabeling. VGAT labeled most amacrine cell dendrites and showed no difference between wt and CNGA3$^{-/-}$Rho$^{-/-}$ retina. (**F**) Electron micrograph of CNGA3$^{-/-}$Rho$^{-/-}$ retina showing a classic example of a conventional synapse of an amacrine cell (AC) onto a postsynaptic process. Scale bar: (**A**, **B**) 33 μm; (**C**) 12 μm; (**E**) 22 μm; (**D**, **F**) 0.5 μm.

Because of the absence of any light-driven photoreceptor input, the CNGA3$^{-/-}$Rho$^{-/-}$ mouse may furthermore be a good model to answer the question of functional integration of retinal transplants. So far, most transplantation studies have used the *rd* mouse model. Gouras and Tanabe[36] showed that in 1-month-old *rd* mice, retinal transplants of neonatal microaggregates exhibit development of photoreceptors with outer segments and that such transplants survive well for at least 8 months, but they found only rare examples of possible synaptic contacts between transplants and host retina. One explanation of the absence of functional integration may be the reduced ability of mature host retinal neurons to form new synapses. However, in various animal models ectopic synaptogenesis takes place in mature retina.[31,32,37] Another reason for missing functional integration may be the dramatic changes of second-order neurons that have been observed in 1-month-old *rd* retinas.[3,4] Retinal degeneration is very fast in the *rd* mouse, with active photoreceptor loss occurring in parallel with the development of the retina, whereas in the CNGA3$^{-/-}$Rho$^{-/-}$ mouse, retinal maturation appears normal and photoreceptor degeneration is significantly delayed compared with that of the *rd* retina. The lack of functional photoreceptor output is obviously not equal to the lack of photoreceptor cells, and their presence is evidently enough to lead to the formation of a normal stratification pattern within the retina.

Given that morphologic alterations in second-order neurons appear much later in the CNGA3$^{-/-}$Rho$^{-/-}$ retina than in the fast-degenerating *rd* retina, the CNGA3$^{-/-}$Rho$^{-/-}$ mouse may turn out to be a better model to study the feasibility of retinal transplantation.

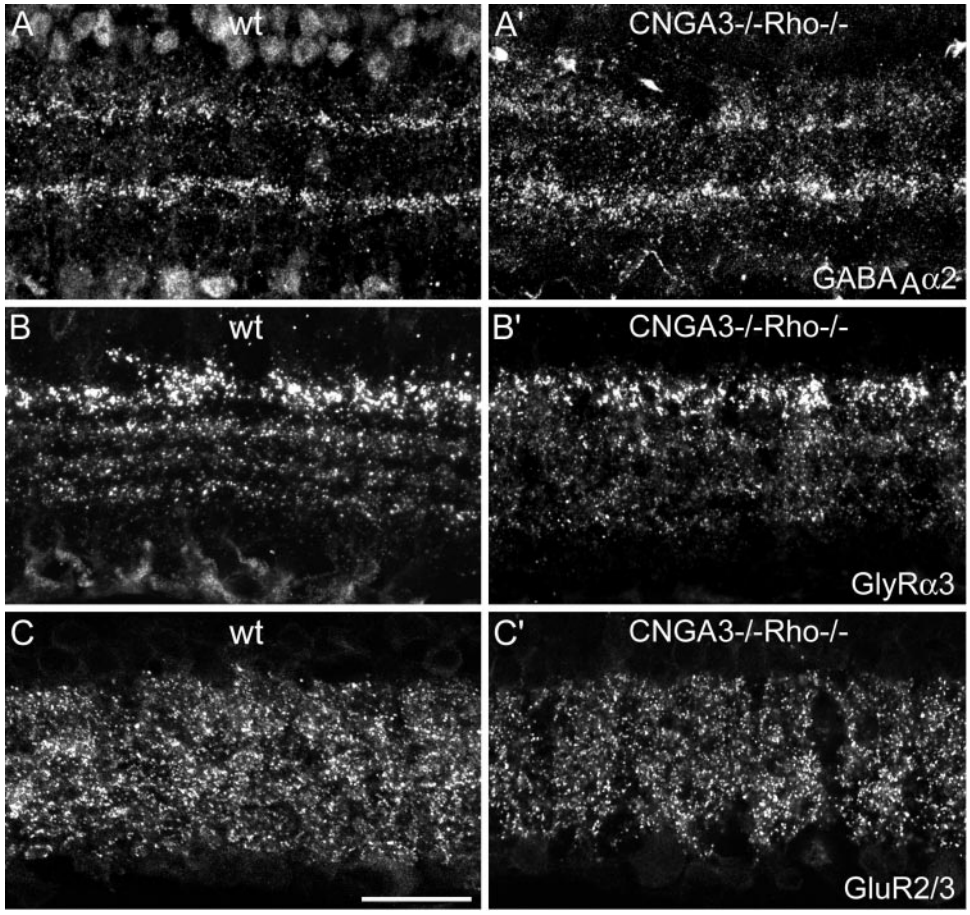

FIGURE 9. Distribution of different transmitter receptor subunits in the IPL of wt (**A**–**C**) and CNGA3$^{-/-}$ Rho$^{-/-}$ (**A′**–**C′**) retinas at Pm12. (**A**, **A′**) Confocal micrographs of vertical sections labeled for the α2 subunit of the $GABA_A$ receptor. Characteristic punctate labeling with an aggregation in two bands was found in both wt and mutant mice. Extrasynaptic labeling of cells in the INL and GCL was restricted to the wt. (**B**, **B′**) The GlyR α3 subunit shows punctate immunofluorescence in four characteristic bands in both wt and mutant mice. (**C**,**C′**) The GluR2/3 subunit shows similar punctate labeling in the IPL of wt and CNGA3$^{-/-}$Rho$^{-/-}$ retinas, except for the innermost IPL, where GluR2/3 receptors were clustered at the terminals of the rod bipolar cells in wt retina but were not so dense in the mutant. Scale bar, 20 μm.

Acknowledgments

The authors thank Walter Hofer and Gong-Sun Nam for excellent technical assistance and Krishna Ghosh and Heinz Wässle for reading and improving the manuscript.

References

1. Bowes C, Li T, Danciger M, Baxter LC, Applebury ML, Farber DB. Retinal degeneration in the rd mouse is caused by a defect in the beta subunit of rod cGMP-phosphodiesterase. *Nature*. 1990;347:677–680.
2. Carter-Dawson LD, LaVail MM, Sidman RL. Differential effect of the rd mutation on rods and cones in the mouse retina. *Invest Ophthalmol Vis Sci*. 1978;17:489–498.
3. Strettoi E, Pignatelli V. Modifications of retinal neurons in a mouse model of retinitis pigmentosa. *Proc Natl Acad Sci USA*. 2000;97:11020–11025.
4. Strettoi E, Porciatti V, Falsini B, Pignatelli V, Rossi C. Morphological and functional abnormalities in the inner retina of the rd/rd mouse. *J Neurosci*. 2002;22:5492–5504.
5. Humphries MM, Rancourt D, Farrar GJ, et al. Retinopathy induced in mice by targeted disruption of the rhodopsin gene. *Nat Genet*. 1997;15:216–219.
6. Lem J, Krasnoperova NV, Calvert PD, et al. Morphological, physiological, and biochemical changes in rhodopsin knockout mice. *Proc Natl Acad Sci USA*. 1999;96:736–741.
7. Jaissle GB, May CA, Reinhard J, et al. Evaluation of the rhodopsin knockout mouse as a model of pure cone function. *Invest Ophthalmol Vis Sci*. 2001;42:506–513.
8. Kaupp UB, Seifert R. Cyclic nucleotide-gated ion channels (review). *Physiol Rev.* 2002;82:769–824.
9. Biel M, Seeliger M, Pfeifer A, et al. Selective loss of cone function in mice lacking the cyclic nucleotide-gated channel CNG3. *Proc Natl Acad Sci USA.* 1999;96:7553–7557.
10. Seeliger MW, Grimm C, Ståhlberg F, et al. New views on RPE65 deficiency: the rod system is the source of vision in a mouse model of Leber congenital amaurosis. *Nat Genet*. 2001;29:70–74.
11. Brandstätter JH, Fletcher EL, Garner CC, Gundelfinger ED, Wässle H. Differential expression of the presynaptic cytomatrix protein bassoon among ribbon synapses in the mammalian retina. *Eur J Neurosci*. 1999;11:3683–3693.
12. Hack I, Frech M, Dick O, Peichl L, Brandstätter JH. Heterogeneous distribution of AMPA glutamate receptor subunits at the photoreceptor synapses of rodent retina. *Eur J Neurosci*. 2001;13:15–24.
13. Nomura A, Shigemoto R, Nakamura Y, Okamoto N, Mizuno N, Nakanishi S. Developmentally regulated postsynaptic localization of a metabotropic glutamate receptor in rat rod bipolar cells. *Cell*. 1994;77:361–369.
14. Vardi N, Morigiwa K. ON cone bipolar cells in rat express the metabotropic receptor mGluR6. *Vis Neurosci*. 1997;14:789–794.
15. Morgans CW. Localization of the alpha(1F) calcium channel subunit in the rat retina. *Invest Ophthalmol Vis Sci*. 2001;42:2414–2418.
16. Krizaj D, Demarco SJ, Johnson J, Strehler EE, Copenhagen DR. Cell-specific expression of plasma membrane calcium ATPase isoforms in retinal neurons. *J Comp Neurol*. 2002;451:1–21.
17. Haverkamp S, Wässle H. Immunocytochemical analysis of the mouse retina. *J Comp Neurol*. 2000;424:1–23.
18. Muresan V, Lyass A, Schnapp BJ. The kinesin motor KIF3A is a component of the presynaptic ribbon in vertebrate photoreceptors. *J Neurosci*. 1999;19:1027–1037.
19. Rice DS, Curran T. Disabled-1 is expressed in type AII amacrine cells in the mouse retina. *J Comp Neurol*. 2000;424:327–338.

20. Haeseleer F, Sokal I, Verlinde CL, et al. Five members of a novel Ca(2+)-binding protein (CABP) subfamily with similarity to calmodulin. *J Biol Chem*. 2000;275:1247–1260.
21. Haverkamp S, Ghosh KK, Hirano AA, Wässle H. Immunocytochemical description of five bipolar cell types of the mouse retina. *J Comp Neurol*. 2003;455:463–476.
22. Cueva JG, Haverkamp S, Reimer RJ, Edwards R, Wässle H, Brecha NC. Vesicular gamma-aminobutyric acid transporter expression in amacrine and horizontal cells. *J Comp Neurol*. 2002;445:227–237.
23. Sosula L, Glow PH. Increase in number of synapses in the inner plexiform layer of light deprived rat retinae: quantitative electron microscopy. *J Comp Neurol*. 1971;141:427–451.
24. Fisher LJ. Development of retinal synaptic arrays in the inner plexiform layer of dark-reared mice. *J Embryol Exp Morphol*. 1979;54:219–227.
25. Kirsch J, Betz H. Glycine-receptor activation is required for receptor clustering in spinal neurons. *Nature*. 1998;392:717–720.
26. Craig AM. Activity and synaptic receptor targeting: the long view. *Neuron*. 1998;21:459–462.
27. Haverkamp S, Müller U, Harvey K, Harvey RJ, Betz H, Wässle H. Diversity of glycine receptors in the mouse retina: localization of the alpha3 subunit. *J Comp Neurol*. 2003;465:524–539.
28. Jones BW, Watt CB, Frederick JM, et al. Retinal remodeling triggered by photoreceptor degenerations. *J Comp Neurol*. 2003;464:1–16.
29. Jansen HG, Sanyal S. Development and degeneration of retina in rds mutant mice: electron microscopy. *J Comp Neurol*. 1984;224:71–84.
30. Jansen HG, Sanyal S. Synaptic changes in the terminals of rod photoreceptors of albino mice after partial visual cell loss induced by brief exposure to constant light. *Cell Tissue Res*. 1987;250:43–52.
31. Dick O, tom Dieck S, Altrock WD, et al. The presynaptic active zone protein bassoon is essential for photoreceptor ribbon synapse formation in the retina. *Neuron*. 2003;37:775–786.
32. Lewis GP, Linberg KA, Fisher SK. Neurite outgrowth from bipolar and horizontal cells after experimental retinal detachment. *Invest Ophthalmol Vis Sci*. 1998;39:424–434.
33. Marc RE, Jones BW, Watt CB, Strettoi E. Neural remodeling in retinal degeneration. *Prog Retin Eye Res*. 2003;22:607–655.
34. Bennett J. Gene therapy for retinitis pigmentosa (review). *Curr Opin Mol Ther*. 2000;2:420–425.
35. Lund RD, Kwan AS, Keegan DJ, Sauve Y, Coffey PJ, Lawrence JM. Cell transplantation as a treatment for retinal disease. *Prog Retin Eye Res*. 2001;20:415–449.
36. Gouras P, Tanabe T. Survival and integration of neural retinal transplants in rd mice. *Graefes Arch Clin Exp Ophthalmol*. 2003;241:403–409.
37. Peng YW, Hao Y, Petters RM, Wong F. Ectopic synaptogenesis in the mammalian retina caused by rod photoreceptor-specific mutations. *Nat Neurosci*. 2000;3:1121–1127.
38. Filoteo AG, Elwess NL, Enyedi A, Caride A, Aung HH, Penniston JT. Plasma membrane Ca2+ pump in rat brain: patterns of alternative splices seen by isoform-specific antibodies. *J Biol Chem*. 1997;272:23741–23747.
39. Howell BW, Gertler FB, Cooper JA. Mouse disabled (mDab1): a Src binding protein implicated in neuronal development. *EMBO J*. 1997;16:121–132.
40. Marksitzer R, Benke D, Fritschy JM, Trzeciak A, Bannwarth W, Möhler H. GABAA-receptors: drug binding profile and distribution of receptors containing the alpha 2-subunit in situ. *J Recept Res*. 1993;13:467–477.